

Computer-assisted Detection and Grading of Prostatic Cancer in Biopsy Image

Shao-Kuo Tai, Yen-Chih Wu, Cheng-Yi Li, Yee-Jee Jan and Shu-Chuan Lin

Abstract—Prostatic biopsies provide abundant information for diagnosis of prostatic cancer. Whereas, inspection in the vast biopsy images under the microscope is a heavy loading to pathologists. Besides, human grading is always subjective to inter- and intra-observer variability. Automatic inspection for prostatic biopsy image is thus necessary. In this paper, we proposed a novel approach to automatically detect prostatic cancer and grade them according to Gleason grading system. The proposed approach contains two stages. First stage is to divide biopsy images into regions and classify these regions into clusters based on their Skeleton-set (SK-set), and each region in the same cluster consists of the similar two-tone texture. In the second stage, multiple Fractal-dimension-based (FD) features extracted from regions are used to analyze the variations of intensity and texture complexity in the boxes with different size. Each region is classified to appropriate grade by using Bayes classifiers, respectively. The leaving-one-out approach is used to estimate error rate. The present experimental results demonstrated that 94.88% of accuracy for a set of 1182 pathological images.

Index Terms—Gleason grading system, Fractal dimension, Skeleton-set, Prostatic cancer.

I. INTRODUCTION

Prostatic cancer is a cancer of the prostatic gland, more than 200,000 American men are diagnosed with prostatic cancer, and nearly 30,000 die from this disease [1]. For confirming the diagnosis of malignancy and guiding treatment, biopsy of the prostate is a key step. By viewing the microscopic image of biopsy specimens, pathologists can determine the histological grade. The prostatic cancer may be distinguished into five grades in Gleason grading system [7]. Figure 1 is the five basic tissue patterns of the classic Gleason grading diagram. Figure 2 shows pathological images of prostatic carcinoma from well differentiated (grade 2) to poor differentiated (grade 5) in our image set. The biopsy Gleason

score is a sum of the primary grade that represents the most common tumor and a secondary grade that represents the second most common tumor, and is a number ranging from 2 to 10 [7].

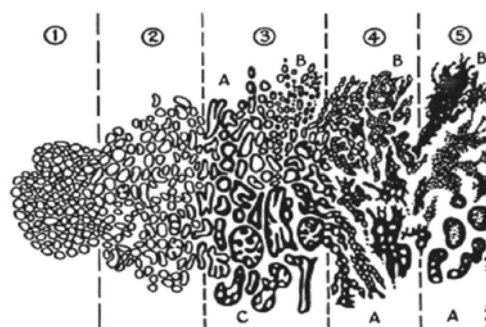


Figure 1. The Gleason grading diagram.

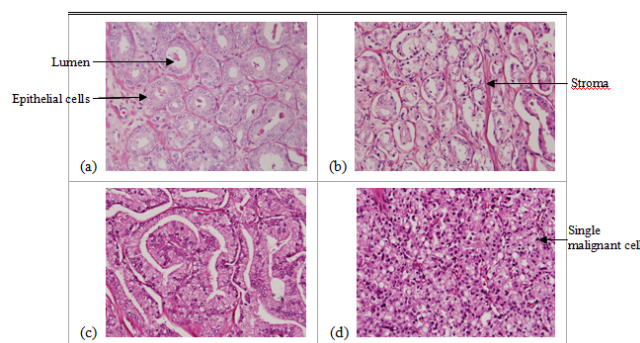


Figure 2. The prostate images of different cancer grades. (a) Gleason grade 2. (b) Gleason grade 3. (c) Gleason grade 4. (d) Gleason grade 5.

Although pathologists will know that how aggressive the cancer is likely to be and how quickly it may spread from the result of Gleason score, human visual grading is time-consuming and very subjective due to variations between interobserver and intraobserver. Therefore, how to use a computer-aided technique to grade prostatic carcinoma automatically is a topic that one should not ignore. Several methods have been proposed for analyzing pathological images of prostate during the last few years. Stotzka et al. [14] proposed neural network and statistical classification methods to distinguish moderately and poorly differentiated lesions of the prostate. The statistical and structural features are extracted from the spatial distribution of epithelial nuclei over the image area, but the authors have described no algorithm for segmenting the epithelial nuclei [3]. Wetzel et al. [2] proposed methods for content based image retrieval to

This work was supported by National Science Council under Grant NSC 98-2221-E-324-032.

Shao-Kuo Tai Author is with the Chaoyang University of Technology, Wufong Township Taichung County, 41349 Taiwan (R.O.C.). Phone: 886-4-23323000 ext 4748; fax: 886-4-23742337; e-mail: sgdai@cyut.edu.tw.

Yen-Chih Wu is with the Chaoyang University of Technology, Wufong Township Taichung County, 41349 Taiwan (R.O.C.). E-mail: s9714601@cyut.edu.tw.

Cheng-Yi Li is with the Chaoyang University of Technology, Wufong Township Taichung County, 41349 Taiwan (R.O.C.). E-mail: s9814606@cyut.edu.tw.

Yee-Jee Jan is with the Department of Pathology, Taichung Veterans General Hospital, Taichung, Taiwan (R.O.C.). E-mail: yejan@vghtc.gov.tw.

Shu-Chuan Lin is with the Department of Pathology, Taichung Veterans General Hospital, Taichung, Taiwan (R.O.C.). E-mail: sara@vghtc.gov.tw.

assist pathology diagnosis. They used Gleason grading of prostate tumor samples as an initial domain for evaluating the effectiveness of the method for specific tasks. Smith et al. [21] proposed a similarity measurement method based on Fourier transform and principle component analysis for Gleason grading of histological slides of prostatic cancer. Jafari-Khouzani et al. proposed a computerized method for grading the pathological images of prostate biopsy samples [9]. In their method, energy and entropy features are calculated from multiwavelet coefficients of an image. These multiwavelet features are tested by using k-nearest-neighbor classifier and leave-one-out approach is used to estimate error rate. Their image set consisted of 100 prostate images of grades 2-5. These methods described above work only when their input images contain only one grade of prostatic cancer, so they cannot detect prostatic cancer from the biopsy images.

The goal of this paper is to propose an automated system to detect prostatic cancer from biopsy images and provide the grade of them according to Gleason grading system. Due to Gleason grading system mainly based on the texture formed by gland and the lumens are the main part of the gland which exhibit white shapes in the biopsy image. So that texture of the lumen is very important for the grading. Beside lumens, the arrangement and intensity of epithelial nuclei also have a considerable impact on grading. For example, if these epithelial nuclei appear in image randomly then it likely to be classified as grade 5. In this paper we consider these two factors individually. First, we apply the features extracted from Skeleton-set of the white shapes to divide images into regions, and classify these regions into clusters. Regions belong to the same cluster have similar texture pattern of lumen. Consequently features extracted from images of the same cluster have rule out the effect of the texture of the lumen. Therefore, in the second stage, we extracted texture feature from gray images to train classifier for each cluster. By means of these classifiers, we can determine the grade of these segmented regions. Since these two factors will not interfere with each other, we can achieve higher precision for the prostatic cancer grade of pathological biopsies. The texture features of gray images used in this study are fractal dimension (FD). The concept of fractal dimension is popular in texture analysis because of providing a proper mathematical framework to study the complex and irregular structure of phenomena in nature. In physical phenomena, the arterial and bronchial trees and the growth of cancers show the features of fractal, and the fractal theory has already provided clinically useful information to discriminate pathological tissue from healthy tissue [8], [18]. For the reason mentioned above, this paper proposed multiple FD-based features which combine the differential box-counting [11] and the proposed entropy-box-counting (EBC) [17] methods to analyze pathological images of prostatic carcinoma. Then, the Bayes classifier is used to classify each image and the leaving-one-out approach is applied to estimate error rate.

This paper is organized as follows. Image segmentation and clustering are introduced in the next section. Extraction and classification of fractal dimension features are presented in Section 3. The experimental results are presented in

Sections 4, respectively. Finally, Section 5 contains conclusions.

II. IMAGE SEGMENTATION AND CLUSTERING BASED ON SK-SET

Other than glands, biopsy images also include many different components, and present complex formation. To segment by pure texture features is very time-consuming and it cannot distinguish all the cases it might encounter. Furthermore, statistic texture features derived from the whole image can be very much influenced by the portion of lumens or other white shapes and ignore other feature. Therefore, it is possible to increase the specificity of texture features by controlling the types of white shapes. For this reason, we will divide an image into regions and clustering these regions based on the pattern of white shapes.

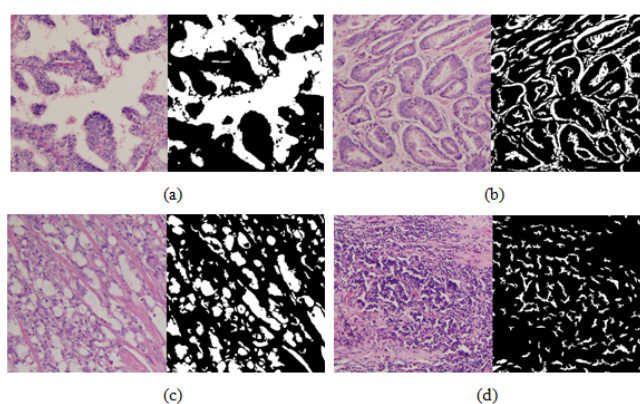


Figure 3. The white shapes in prostatic biopsy image.

There are three major colors in prostatic biopsy images, which are white, red and blue. Besides lumens of prostatic gland and fat, white shapes in prostatic biopsy images can also be caused by the process of biopsy preparation. As show in figure 3, (a) is the normal prostate; (b), (c), and (d) is the grade 3, 4, and 5 respectively, where (c) contains some fat. The white shapes in these images represent the types of gland. Different size, density and shape mean different patterns of gland. Therefore, we adopt three important criteria to distinguish them. In this paper, we extracted Skeleton-set to represent these three criteria. Skeleton-set is described as below.

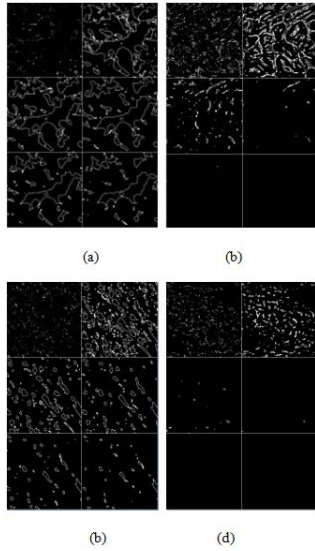


Figure 4. SK-set of images in figure 3.

At first, images transform to two-tone model by keeping all the white shapes in image and others regions convert into background, denoted as A_0 . We perform morphological operation to get the skeleton-set. Let B is the structure element, and $A_k = A_{k-1} \ominus B$, $S_k = A_k - A_k \circ B$, where \ominus is erosion and \circ denotes opening. Then we can get SK-set, $\{S_k; k=1$ to $N\}$. It can reveal these three criteria by counting the pixel of S_k . Figure 4 are the SK-set of the images in figure 3, where N is 6 and every picture from top-left to bottom-right is S_1 to S_6 respectively. Figure 4 (a) shows that the pixel number of S_1 is less than others while S_6 is largest, which represent figure 3(a) includes large white shapes. The pixel number of S_3 is much larger than S_4 I Figure 4 (b), which means figure 4 (c) contains band-shape components. In the same way, SK-set in figure 4 (c) and (d) represents figure 3 (c) contains some unequal size components and figure 3(d) contains small but high density components. With the SK-set, we apply split and merge method to divide image into regions and classify them by Bayer classifier.

III. EXTRACTION AND CLASSIFICATION OF FRACTAL DIMENSION FEATURES

The term fractal was coined by Mandelbrot [4], which comes from the Latin word “fractus” and means irregular fragments. Based on the concept of Mandelbrot, many natural objects exhibit fractal property or self-similarity. Self-similarity can be described as follows [11], [12]. A bounded set, A , in Euclidean n -space is self-similar if A is the union of N_r distinct (non-overlapping) copies of itself scaled down by a ratio r . The fractal dimension D of A can be derived from the following basic equation [4]:

$$D = \frac{\log(N_r)}{\log(1/r)} \quad (1)$$

However, natural phenomena or objects do not exhibit deterministic self-similarity in practically due to they can often be classified as random fractals, meaning that each smaller part of it is statistically similar to the whole.

Therefore, an object becomes statistically identical to the original one if it is scaled down by a ratio r in all n dimensions, so that (1) is satisfied [11].

Several approaches exist to estimate the FD of an image. Among several approaches, the DBC method is the most popular for estimating the FD of an image [19], and it is well used in the field of texture analysis due to its computational simplicity [16], [20]. In addition, the method possesses the advantages of simple, accurate, and efficient relative to other box-counting methods [11]. The DBC method is adopted herein because it gives a better approximation for the image intensity surface. In general, compared with the low-grade prostatic carcinoma in pathological image, the high-grade prostatic carcinoma has sharp gray-level variation in neighboring pixels due to sheets of single dark malignant cells invade stroma. Thus, the DBC method can significantly distinguish low-grade and high-grade prostatic carcinoma by measuring the variations of intensity in local regions. Before using the DBC method, the color pathological images of prostatic tissue are transformed into gray-level images by getting R channel from RGB color space for enhancing the contrast between malignant cells and background tissue. In above pre-processing stage, the malignant cells will be darker than other pathological objects because these are stained blue compared to other pathological objects, such as stroma stained red and lumens which do not stain and belong to white in H&E-stained pathological images. The DBC method is described as follows.

Consider that an image of size $M \times M$ pixels has been scaled down to a size $s \times s$, where $1 < s \leq M/2$ and s in an integer. Then, we can get the scale ratio $r = s/M$. Consider the image as a three-dimensional (3-D) space that (x, y) denoting two-dimensional (2-D) position and the third coordinate (z) denoting gray level of an image. The (x, y) space is divided into grids of size $s \times s$. There is a column of boxes of size $s \times s \times h$ on each grid, where $\lfloor G/h \rfloor = \lfloor M/s \rfloor$ and G is the total number of gray levels in an image. Let the maximum and minimum gray level of an image in the (i, j) th grid fall in box number k and l , respectively. The contribution of N_r in the (i, j) th grid is expressed as follows:

$$n_r(i, j) = k - l + 1 \quad (2)$$

After taking contributions from all grids, we can get

$$N_r = \sum_{i,j} n_r(i, j) \quad (3)$$

N_r is counted for different scale ratio r . Then the fractal dimension D can be estimated from the least-squares linear fitting of $\log(N_r)$ versus $\log(1/r)$ by using (1).

For analyzing the texture complexity in pathological images for different Gleason grades of prostate carcinoma, this paper further proposes an EBC method which combines the entropy method with the box-counting method. The

image of 2-D is partitioned into several grids of size $s \times s$. For each grid in the EBC method, we compute its entropy [15], thus the contribution of E_r in the (i, j) th grid is defined as:

$$e_r(i, j) = -\sum_{k=0}^{G-1} p(z_k) \log_2 p(z_k), \quad (4)$$

where Z_k is total number of pixels with gray level k in the (i, j) th grid of an image, and $p(Z_k)$ denotes the probability of occurrence of gray level k in the (i, j) th grid of an image. After taking the summation of the square of each contribution from all grids, we have

$$E_r = \sum_{i,j} e_r(i, j)^2. \quad (5)$$

Then using (1), the fractal dimension D can be estimated from the least-squares linear fitting of $\log(N_r)$ versus $\log(1/r)$. The reason for counting E_r is that we can measure more accurately the variations of texture complexity for the regions with different size, i.e., different values of s .

Voss [13] have showed that different textures may have the same FD. This may be due to natural phenomena usually only exhibit the property of random fractals; in other words, natural phenomena are not self-similarity over all scales [19]. Therefore, for finding distinguishing features, multiple FD-based features are calculated from the regions with different size in this paper, such as the grids with different size. The representation of multiple FD-based features is described as follows:

$$MF = (f_D^i, f_E^i), \quad i = 1, 2, 3, 4 \quad (6)$$

where f_D^i, f_E^i denote the FD of an image calculated from the grids with different size via DBC and EBC methods, respectively; $i = 1$, denotes the grids with different size s ($s = 2, 4$, and 8), $i = 2$, denotes the grids with different size s ($s = 8, 16$, and 32), $i = 3$, denotes the grids with different size s ($s = 32, 64$, and 128), and $i = 4$, denotes the grids with different size s ($s = 2, 4, 8, 16, 32, 64$, and 128). For example, f_E^2 , denotes the FD of an image calculated from the grids with size $8, 16$, and 32 by using EBC method. The total number of features used by this paper is 8.

IV. EXPERIMENTAL RESULTS

In experiment results, the Bayes classifiers and the leave-one-out approach is used to estimate system performance. Furthermore, this paper compared with three multiwavelet features, including GHM [6], CL [5], and SA4 [10] multiwavelets to calculate the error rate. The three multiwavelets above are the first three high on the correct classification rate among all of the multiwavelets in Jafari-Khouzani's method [9].

Table 1. Comparison of our method and multiwavelet methods

	SA-4	CL	GHM	DBC & EBC
CCR without clustering	87.36%	86.81%	87.01%	90.86%
CCR with clustering	91.35%	90.23%	90.98%	94.88%

Table 1 is the correct classification rate (CCR) of our method and multiwavelet based methods. The first row evaluates methods without clustering by the texture of white shapes. Experimental results show that the method based on the FD-based features has 3% higher CCR than multiwavelet based methods. Images used for experiment of second row in table 1 are all clustered by the texture of white shapes. The maximum correct classification rate (CCR) is 94.88% generated by the FD-based features as well and the pre-clustering can increase the CCR about 4%. These experimental results demonstrate that our method can promote significantly the accuracy of classification.

V. CONCLUSION

This paper developed a two-stage automated system for detecting and grading pathological images of prostatic carcinoma. First stage is to divide the image into regions and classify these regions into proper cluster based on SK-set feature. SK-set features derived from the white shapes in images represent the character of lumen. After clustering, every cluster contains the same type of lumen and increases the specificity of the extracted grading feature by narrowing down the possibility of grade of prostatic cancer. In the second stage, the FD-based features are extracted to classify these regions into proper grade. Experimental results demonstrate that our method increases the system performance and achieve the CCR of 94.88%, much better than the only one stage approach.

REFERENCES

- [1] American Cancer Society, *Cancer Facts & Figures 2007*. Atlanta, GA: American Cancer Society, 2007.
- [2] A. W. Wetzel, R. Crowley, S. J. Kim, R. Dawson, L. Zheng, Y. M. Joo, Y. Yagi, J. Gilbertson, C. Gadd, D. W. Deerfield, and M. J. Becich, "Evaluation of prostate tumor grades by content-based image retrieval," *Proceedings of the SPIE on AIPR Workshop Advances in Computer-Assisted Recognition*, vol. 3584, pp. 244-252, Washington, DC, 1999.
- [3] A. Tabesh, V. Kumar, H. Pang, D. Verbel, A. Kotsianti, M. Teverovskiy, and O. Saidi, "Automated prostatic cancer diagnosis and gleason grading of tissue microarrays," *Proceedings of the SPIE on Medical Imaging*, vol. 5747, pp. 58-70, April 2005.
- [4] B. B. Mandelbrot, *Fractal Geometry of Nature*. San Francisco, CA: Freeman, 1982.
- [5] C. K. Chui and J. A. Lian, "A study of orthonormal multiwavelets," *Appl. Numer. Math.*, vol. 20, pp. 273-298, 1995.
- [6] E. Gose, R. Johnsonbaugh, and S. Jost, *Pattern Recognition and Image Analysis*. Englewood Cliffs, NJ: Prentice-Hall, 1996.
- [7] G. J. O'Dowd, R. W. Veltri, M. C. Miller, and S. B. Strum, "The Gleason Score: A Significant Biologic Manifestation of Prostatic cancer Aggressiveness on Biopsy," *Prostatic cancer Research Institute: PCRI Insights*, vol. 4, no.1, pp. 1-5, 2001.

- [8] J. W. Baish and P. K. Jain, "Fractals and cancer," *Cancer Research*, vol. 60, pp. 3683-3688, 2000.
- [9] K. Jafari-Khouzani and H. Soltanian-Zadeh, "Multiwavelet grading of pathological images of prostate," *IEEE Transactions on Biomedical Engineering*, vol. 50, no. 6, pp. 697-704, June 2003.
- [10] L.-X. Shen, H. H. Tan, and J. Y. Tham, "Symmetric-antisymmetric orthonormal multiwavelets and related scalar wavelets," *Appl. Computational Harmonic Anal. (ACHA)*, vol. 8, no. 3, pp. 258-279, May 2000.
- [11] N. Sarkar and B. B. Chaudhuri, "An efficient differential box-counting approach to compute fractal dimension of image," *IEEE Transactions on Systems, Man and Cybernetics*, vol. 24, no. 1, pp. 115-120, Jan 1994.
- [12] B.B. Chaudhuri, N. Sarkar, "Texture segmentation using fractal dimension," *IEEE Transactions on Pattern Analysis and Machine Intelligence*, vol. 17, no. 1, 1995.
- [13] R. F. Voss, "Random fractals: Characterization and measurement." In: R. Pynn and A. Skjeltorp, Ed., *Scaling Phenomena in Disorderd Systems*, Plenum, New York, 1986.
- [14] R. Stotzka, R. Männer, P. H. Bartels, and D. Thompson, "A hybrid neural and statistical classifier system for histopathologic grading of prostate lesions," *Analytical Quantitative Cytol. Histol.*, vol. 17, no. 3, pp. 204-218, 1995.
- [15] R. C. Gonzalez, R. E. Woods, *Digital Image Processing*, 2nd ed. New Jersey: Prentice-Hall, 2002.
- [16] S. Yan, L. Jianming and Y. Takashi, "Texture classification for liver tissues from ultrasonic B-scan images using testified PNN," *IEICE Transactions on Information and Systems*, vol. 89, no. 8, pp. 2420-2428, 2006.
- [17] Shou-Kuo Dai, Chin-Ling Ho, Yee-Jee Jan, Shu-Jiuan Lin, "Texture Analysis and Classification of Pathological images for Automatic Grading of Prostatic Carcinoma," The 19th International Conference on Information Management.
- [18] T., Takahashi, T. Murata, k. Narita, T. Hamada, H. Kosaka, M. Omori, K. Takahashi, H. Kimura, H. Yoshida, and Y. Wada, "Multifractal analysis of deep white matter microstructural changes on MRI in relation to early-stage atherosclerosis," *NeuroImage*, vol. 32, no. 3, pp. 1158-1166, 2006.
- [19] T. Stojic, I. Reljin, and B. Reljin, "Adaptation of multifractal analysis to segmentation of microcalcifications in digital mammograms," *Physica A*, vol. 367, pp. 494-508, 2006.
- [20] W.-Li Lee, Y.-Chang Chen, and K.-Sheng Hsieh, "Ultrasonic liver tissues classification by fractal feature vector based on M-band wavelet transform," *IEEE Transactions on Medical Imaging*, vol. 22, no. 3, pp. 382-392, March 2003.
- [21] Y. Smith, G. Zajicek, M. Werman, G. Pizov, and Y. Sherman, "Similarity measurement method for the classification of architecturally differentiated images," *Computers and Biomedical Research*, vol. 32, no. 1, pp. 1-12, 1999.